Chemical Geology 627 (2023) 121457

Contents lists available at ScienceDirect

Chemical Geology

journal homepage: www.elsevier.com/locate/chemgeo

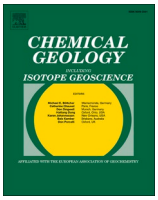

A new procedure for separating thallium from geological materials prior to stable isotope ratio determination by MC–ICP–MS

Zhao-Yang Wang [a,b,c], Jie Li [a,b,*], Lu Yin [d], Le Zhang [a,b], Jun-Jie Liu [a,b], Neng-Ping Shen [e], Shuang Yan [b,f], Qing-Dian Guan [g]

[a] State Key Laboratory of Isotope Geochemistry, Guangzhou Institute of Geochemistry, Chinese Academy of Sciences, Guangzhou 510640, China
[b] CAS Center for Excellence in Deep Earth Science, Guangzhou 510640, China
[c] College of Earth and Planetary Sciences, University of Chinese Academy of Sciences, Beijing 100101, China
[d] Hebei Key Laboratory of Strategic Critical Mineral Resources, Hebei GEO University, Shijiazhuang 050031, China
[e] State Key Laboratory of Ore Deposit Geochemistry, Institute of Geochemistry, Chinese Academy of Sciences, Guiyang 550081, China
[f] CAS Key Laboratory of Mineralogy and Metallogeny, Guangzhou Institute of Geochemistry, Chinese Academy of Sciences, Guangzhou 510640, China
[g] Guizhou Tongwei Analytical Technology Co., Ltd., Guiyang 550025, China

ARTICLE INFO

Editor: Michael E. Boettcher

Keywords:
Tl isotopes
Two-stage tandem column separation
TBP resin
AG50W-X12 ion-exchange resin
MC–ICP–MS

ABSTRACT

In this paper, a simple and efficient method is presented for the separation of Tl from various complex geological samples and subsequent accurate and precise Tl isotope measurements by multi-collector inductively coupled plasma–mass spectrometry (MC–ICP–MS). Chemical separation involves a two-stage tandem column method with tributyl phosphate (TBP) extraction resin and AG50W-X12 cation ion-exchange resin, which efficiently separate Tl from the matrix, interfering elements, and sulfate ions. External normalization to NIST SRM 981 Pb and standard–sample bracketing using NIST SRM 997 Tl were utilized for the instrumental mass bias correction. The $\varepsilon^{205}Tl_{NIST\ 997}$ data are reported as the per 10^4 deviation of $^{205}Tl/^{203}Tl$ from NIST SRM997 (Rehkämper and Halliday, 1999; Vaněk et al., 2016). The overall external precision for the $\varepsilon^{205}Tl_{SRM\ 997}$ values is estimated to be ±0.6 (2SD; $n > 1000$) and ± 0.8 (2SD; $n = 5$) based on repeated analyses of NIST SRM 997 and the geological reference material NOD-A-1, respectively. The Tl isotopic compositions of nine well-documented geological reference materials are in good agreement with the values reported in previous studies, confirming the validity of our new analytical procedure for the accurate determination of Tl stable isotopic compositions of geological samples.

1. Introduction

Thallium (Tl) belongs to 13th Group of the Periodic Table of the Elements sitting between mercury (Hg) and lead (Pb). It has been identified to be a non-essential and extremely toxic metal, far exceeding the toxicity of Pb, Cd, and Hg (Feldman and Levisohn, 1993; Karbowska, 2016; Kazantzis, 2000; Peter and Viraraghavan, 2005). The geochemistry of Tl is complex (Shaw, 1952; Vaněk et al., 2009). Thallium is present in nature mainly as Tl^{3+} and Tl^{+}, with the latter is dominant. Monovalent Tl^{+} tends to behave as a lithophile element similar to K, but also exhibits chalcophile behavior and bonds with S in inorganic and organic compounds (Jones et al., 1993; Kiseeva and Wood, 2013; Nielsen et al., 2011; Nielsen et al., 2014; Wood et al., 2008). Thallium in the environment is mainly derived by weathering of K-rich rocks and sulfide minerals (Vaněk et al., 2009; Voegelin et al., 2015). The concentrations of Tl in non-contaminated soils and sediments are normally at or below the μg/g level. Thallium tends to occur in K-rich igneous rocks, in which the similar ionic radii of K and Rb allow the substitution of K^{+} or Rb^{+} with Tl^{+}, and in soils proximal to sulfide deposits (Brett et al., 2018; Nielsen et al., 2017; Xiao et al., 2004). The release of anthropogenic Tl into the environment occurs mainly through mining and industrial activities. Industrial sources are estimated to emit 2000–5000 tons of Tl per year as vapor, dust, fluids, and solids (Karbowska, 2016; Liu et al., 2017; Liu et al., 2020; Vaněk et al., 2018; Vaněk et al., 2016; Wang et al., 2018; Xu et al., 2018), which leads to significant negative environmental and ecological effects. As such, more research is required to better

* Corresponding author at: State Key Laboratory of Isotope Geochemistry, Guangzhou Institute of Geochemistry, Chinese Academy of Sciences, Guangzhou 510640, China.
E-mail address: jieli@gig.ac.cn (J. Li).

https://doi.org/10.1016/j.chemgeo.2023.121457
Received 3 January 2023; Received in revised form 17 March 2023; Accepted 29 March 2023
Available online 2 April 2023

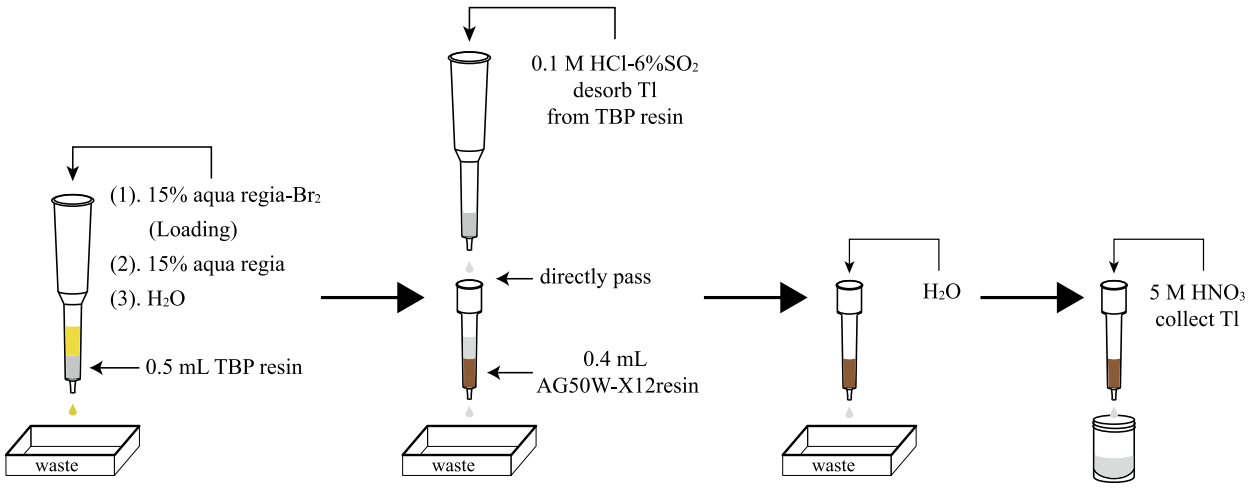

Fig. 1. Two-stage tandem column setup for Tl separation. Details of the Tl separation procedure can be seen in Table 1 and Fig. 3.

constrain the anthropogenic effects on the biogeochemical cycleing of Tl.

Advances in multi-collector inductively coupled plasma mass spectrometry (MC–ICP–MS) technology mean Tl isotopic fractionation can be used as a tool to better understand the geochemical behavior of Tl and trace contamination sources (Liu et al., 2020; Nielsen et al., 2006b; Nielsen et al., 2017; Ostrander et al., 2019; Rehkämper et al., 2004; Rehkämper and Halliday, 1999; Vaněk et al., 2018; Vaněk et al., 2016). Thallium has two naturally occurring stable isotopes, ^{203}Tl (29.46%) and ^{205}Tl (70.54%). Given that the relative mass difference between the two stable isotopes of Tl is <1%, and the magnitude of mass-dependent stable isotopic fractionation due to kinetic and equilibrium processes scales inversely with both the overall and relative mass differences (Bigeleisen and Mayer, 1947), it was assumed there would be little mass-dependent Tl isotopic fractionation in nature. However, meteorite samples exhibit large Tl isotopic variations of about 50 ε^{205}Tl units ($\varepsilon^{205}Tl = [(^{205}Tl/^{203}Tl)_{sample} / (^{205}Tl/^{203}Tl)_{standard} - 1] \times 10{,}000$, Nielsen et al. (2006a)). This large isotopic fractionation reflects the highly volatile and labile cosmochemical nature of Tl, and the radiogenic decay of extinct ^{205}Pb (half-life ~15 Myr) to ^{205}Tl. Highly fractionated Tl isotopic compositions have also been documented in low-temperature-altered oceanic crust ($\varepsilon^{205}Tl \sim -20$) and marine ferromanganese sediments ($\varepsilon^{205}Tl \sim +15$) (Howarth et al., 2018; Nielsen et al., 2006b; Nielsen et al., 2017; Rehkämper et al., 2002). Recently, Tl stable isotopes have been used to assess different environmental processes related to immobilization or plant uptake of Tl (Kersten et al., 2014; Vaněk et al., 2018; Vejvodová et al., 2022; Vejvodová et al., 2020).

Previous studies of the Tl isotopic systematics of geological materials were conducted by MC–ICP–MS using a combination of Pb (NIST SRM 981 Pb) doping and standard–sample bracketing methods to correct instrumental mass bias. With this approach, a precision of 0.2–0.7 ε^{205}Tl units can be achieved (Brett et al., 2018; Nielsen et al., 2015; Nielsen et al., 2017; Ostrander et al., 2017; Wang et al., 2022a). The method requires that the Pb isotopic composition of the doped sample and standard solution are identical. However, Pb has four naturally occurring isotopes (masses 208, 207, 206, and 204) and ^{208}Pb, ^{207}Pb, and ^{206}Pb are produced by the radioactive decay of ^{232}Th, ^{235}U, and ^{238}U, respectively. As such, the Pb isotopic composition of natural samples varies greatly, and any Pb present in the sample solution before addition of NIST SRM 981 from the sample matrix or contamination can affect the Tl isotopic measurements. Due to the high [Pb]/[Tl] ratios (> 10^3) in most geological samples, it is difficult to completely separate Pb from Tl, which hinders precise and accurate Tl isotopic analysis. Furthermore, Tl isotope ratio measurements by MC–ICP–MS can be compromised by analytical artefacts due to spectral interferences and matrix effects, include molecules isobaric interferences and result offset due to residual sample matrix (Nielsen et al., 2004; Nielsen et al., 2017). Therefore, separation of Tl from the sample matrix is critical for accurate Tl isotope ratio determinations. The two-stage ion-exchange chromatographic method using AG1-X8 resin initially developed by Rehkämper and Halliday (1999) has been widely used for separation of Tl from geological samples. The original method has been modified slightly but the procedures remain unchanged (Baker et al., 2009; Brett et al., 2018; Nielsen et al., 2004; Nielsen et al., 2007). The separation technique is based on the fact that Tl^{3+} forms anionic complexes in acidic solutions (e.g. $TlCl_6^{3-}$ or $TlBr_6^{3-}$) and partitions very strongly onto the anion ion-exchange resin while Tl^+ does not. Therefore, Tl can be stripped from the resin by elution with a reducing solution (SO_2 dissolved in 0.1 M HCl) that converts Tl^{3+} to Tl^+. The method separates Tl from geological samples effectively but bothers from the SO_4^{2-} (that formed by the oxidation of SO_2 used during collection of Tl). Nielsen et al. (2004) demonstrated that the presence of H_2SO_4 in sample solutions can result in analytical artefacts. To eliminate this matrix effect, an appropriate amount of H_2SO_4 was added to the Tl standard solution and samples to matrix match the samples and standards. Recent studies have used a single column with AG1-X8 resin to separate Tl from geological samples with high Tl concentrations (Ostrander et al., 2017; Wang et al., 2022b).

In this study, a two-stage tandem column protocol was developed using tributyl phosphate (TBP) resin and AG50W-X12 cation ion-exchange resin to cleanly separate Tl from geological samples for precise isotopic measurements by MC–ICP–MS. In this procedure, Tl^{3+} was absorbed onto a small volume (0.5 mL) of TBP resin in 15% aqua regia and stripped from the resin by 0.1 M HCl-6% *w/w* SO_2, which was then directly eluted onto AG50W-X12 resin (0.4 mL) to remove sulfur compounds. This method has a high efficiency and recovery (> 98%) and low blank (< 2 pg), and completely avoids the effects of SO_4^{2-} and residual Pb during the mass spectrometric measurements. The protocol was validated by analysis of the Tl isotopic compositions of nine geological reference materials.

2. Experimental

2.1. Reagents and materials

To reduce the risk of Pb contamination from the experimental environment and reagents, all procedures were carried out in the Class 100 clean laboratory at the State Key Laboratory of Isotope Geochemistry, Guangzhou Institute of Geochemistry, Chinese Academy of Science (GIG-CAS), Guangzhou, China, and Guizhou Tongwei Analytical Technology Company Limited, Guiyang, China. The hydrofluoric acid (HF),

Table 1
The separation processes in this study and the other purification method for comparison (take Nielsen et al. (2004) as an example).

Method	Stage	Resin	Purpose	Step	Volume (mL)
Nielsen et al. (2004)	First	AG1-X8 (1.5 mL 200–400 mesh)	Condition	0.1 M HCl	10.5
			Condition	0.1 M HCl-1% Br_2	6
			Load sample	0.1 M HCl-0.1% Br_2	
			Matrix removal	0.03 M HBr-0.5 M HNO_3–1%Br_2	15
			Matrix removal	0.03 M HBr-2 M HNO_3–1%Br_2	15
			Matrix removal	0.1 M HCl-1% Br_2	15
			Collection of Tl	0.1 M HCl-5%SO_2	23.5
	Second	AG1-X8 (0.1 mL 200–400 mesh)	Condition	0.1 M HCl	2.5
			Condition	0.2 M HBr-1% Br_2	0.4
			Load sample	0.2 M HBr-5% Br_2	
			Matrix removal	0.03 M HBr-0.5 M HNO_3–1%Br_2	1.5
			Matrix removal	0.03 M HBr-2 M HNO_3–1%Br_2	1.1
			Matrix removal	0.1 M HCl-1% Br_2	1.1
			Collection of Tl	0.1 M HCl-5%SO_2	1.6
This study	First	TBP (0.5 mL 50–100 μm)	Condition	H_2O	4
			Condition	15% aqua regia-3% Br_2	6
			Load sample	15% aqua regia-13% Br_2	3
			Matrix removal	15% aqua regia	12
			Matrix removal	H_2O	2
			Collection of Tl	0.1 M HCl-6%SO_2	12
	Second	AG50W-X12 (0.4 mL 200–400 mesh)	Condition	H_2O	6
			Condition	0.1 M HCl-6%SO_2	2
			Load sample	Tandem column	
			Matrix removal	H_2O	2
			Collection of Tl	5 M HNO_3	2.5

nitric acid (HNO_3), and hydrochloric acid (HCl) were purified twice using a Savillex ™ DST-1000 sub-boiling distillation system (Eden Prairie; MN, USA). Ultrapure water (18.2 MΩ cm^{-1}) was used throughout this study and was produced from a Milli-Q element system (Burlington; MA, USA). The TBP resin (50–100 μm) was obtained from Triskem International (Bruz, France). The AG50W-X12 (200–400 mesh) cation ion-exchange resin was obtained from Bio-Rad Laboratories (Hercules, CA, USA). Saturated bromine (Br_2) water was prepared by equilibration of high-purity Br_2 with ultrapure water. A solution of 0.1 M HCl–6% *w/w* SO_2 was used to elute Tl from the TBP resin. The solution was prepared using the method of Brett et al. (2018). The liquified SO_2 was purchased from GuangQi, Guangdong Province, China. The NIST SRM 997 standard solution was used as the Tl isotope standard. A NIST SRM 981 Pb standard solution was used for external normalization to correct for instrument mass bias. Another Tl standard solution (Fluka; Lot BCBK3320V) was purchased from Honeywell Research Chemicals Limited and used to assess the long-term precision of instruments.

Table 2
Typical instrumental setup during MC-ICP-MS analysis in this study.

Parameter	Neptune Plus	Nu plasma 3
RF power	1200 W	1300
Auxiliary gas (Ar) flow rate	0.98 L min^{-1}	0.85 L min^{-1}
Sample gas (Ar) flow rate	0.975 L min^{-1}	0.753 L min^{-1}
Cooling gas (Ar) flow rate	16 L min^{-1}	13.5 L min^{-1}
Measurement mode	static	static
Interface cones	Jet cone + X cone	Ni Sampler Cone - 1.9 MM Hole + Ni HS1–7 Skimmer cone
Detection system	Faraday cups	Faraday cups
Amplifier	10^{11} Ω	10^{11} Ω
Integration time	4.19 s	5 s
Mass resolution	Low-resolution model	Low-resolution model
Aridus III		
Sweep gas flow rete	2.75	5.36 L min^{-1}
Nitrogen gas	2.6	0.0 mL min^{-1}
Spray chamber temperature	104 °C	110 °C
Desolvator temperature	140 °C	140 °C
Cup configuration	L2 ^{203}Tl / L1 ^{204}Pb / C ^{205}Tl / H1 ^{206}Pb / H2 ^{207}Pb / H3 ^{208}Pb	

2.2. Sample digestion and preparation

Approximately 30–800 mg of reference material powder, depending on the mass fraction of Tl in the sample, was placed in the PFA (Teflon) beakers. The samples were digested with concentrated HNO_3 and HF (the Fe—Mn nodules were dissolved in 6 M HCl) on a hotplate at 120 °C for 2–3 d. The soil and shale samples were digested with concentrated HNO_3 and HF in tightly sealed PFA bomb vials and placed in an oven at 190 °C for 2–3 day. After evaporation to dryness at 120 °C, the samples were dissolved in 3 mL of 15% *v/v* aqua regia and again evaporated to dryness. The samples were redissolved in 1.5 mL of 30% *v/v* aqua regia and diluted with ultrapure water, and then 0.4 mL of saturated Br_2 water was added to the samples. Finally, 3 mL of 15% aqua regia–13% *v/v* Br_2 solution was refluxed at 80 °C for a minimum of 12 h to ensure complete oxidation of Tl to Tl^{3+}. After cooling, the solution was ready to be loaded onto the separation column.

2.3. Chromatographic separation

A two-stage tandem column setup was used to separate Tl from the samples with TBP resin (50–100 μm) and AG50W-X12 cation ion-exchange resin (200–400 mesh) (Fig. 1). The separation schedule is shown in Table 1 and Fig. 3. On the first column, 0.5 mL of TBP resin was loaded into a Bio-Rad column (0.8 cm inner diameter) and pre-cleaned with 4 mL of 0.1 M HCl–6% SO_2 and 4 mL of ultrapure water. The resin was subsequently conditioned with 6 mL of 15% *v/v* aqua regia–3% *v/v* Br_2. The sample solutions were loaded onto the columns and, subsequently, another 12 mL of 15% *v/v* aqua regia was added to elute major and trace elements (e.g., Ti, Mn, Cu, Zn, Ce, and Pb), and 2 mL of ultrapure water was added to elute residual aqua regia. A Bio-Rad column (0.6 cm inner diameter) was used as the second column and was packed with 0.4 mL of AG50W-X12 cation ion-exchange resin. The resin was cleaned three times with 6 mL of 6 M HCl and 6 mL of ultrapure water, and then conditioned with 2 mL of 0.1 M HCl–6% SO_2. Subsequently, the two columns were joined together (the first column at the top; Fig. 1). A solution of 12 mL of 0.1 M HCl–5% *w/w* SO_2 was used to reduce Tl^{3+} to Tl^{+} to enable elution from the first column, which directly passed onto the second column. After completely eluting the Tl, the first column was carefully removed. The sulfur compounds (e.g., SO_4^{2-}, HSO_3^-, SO_2, etc.) are not absorbed while Tl was absorbed in the second column. The second column was eluted with 2 mL of ultrapure water to remove the residual sulfur compounds. Finally, the Tl was collected in 2.5 mL of 5 M HNO_3. The samples were evaporated at 120 °C, and then diluted to 0.5

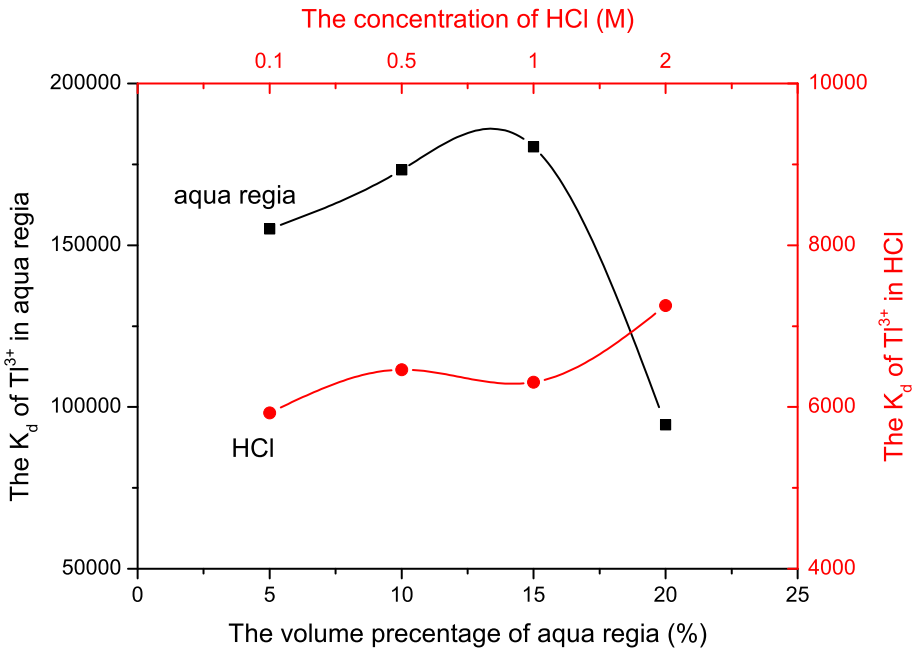

Fig. 2. The distribution coefficient (K_d) of Tl^{3+} on TBP resin in different concentration HCl and aqua regia. (For interpretation of the references to colour in this figure legend, the reader is referred to the web version of this article.)

mL with 2% HNO_3 before being analyzed by MC–ICP–MS.

2.4. Mass spectrometry analysis

During the method development stage of this work, a quadrupole ICP–MS (Thermo Scientific Xseries-2) was used in conventional mode for semi-quantitative and quantitative elemental measurements, such as those of the major matrix elements (Ti, Mn, Fe, etc.), transition metals (Cu, Co, Zn, etc.), rare earth elements (Ce, Pr, Nd, etc.), and Pb. The S was measured by MC–ICP–MS. Details of the analytical methods are given by Sun et al. (2018). Drift corrections were carried out using Rh and Bi as internal standards and by repeatedly analyzing a quality control solution over the duration of a run.

Thallium isotope ratio measurements were carried out with a Neptune Plus MC–ICP–MS (Thermo Scientific) at the CAS Key Laboratory of Mineralogy and Metallogeny, Guangzhou Institute of Geochemistry (GIG), Chinese Academy of Sciences (CAS), Guangzhou, China, and with a Nu Plasma 3 MC–ICP–MS (Nu Instrument) at the Guizhou Tongwei Analytical Technology Company Limited, Guiyang, China. The typical instrumental setup during the MC–ICP–MS analyses is shown in Table 2. Sample solutions were introduced into the plasma using an Aridus (III) desolvator with 100 μL min^{-1} (Neptune Plus) and 50 μL min^{-1} (Nu Plasma 3) PFA nebulizers. The instrument sensitivity of the Neptune Plus and Nu Plasma 3 was about 1.2 and 1.5 V for ^{205}Tl for a 2 ng g^{-1} Tl solution, respectively. Each analysis included 50 cycles of 4.2 s (Neptune Plus) or 5 s (Nu plasma 3) integration time. The injection system was washed out between each of the measurements with 2% HNO_3 to ^{205}Tl signals of <1 mV. An on-peak-zero (OPZ) correction was applied by measuring the intensities of all the masses in the wash solution of 2% HNO_3 before and after every analysis.

External normalization by standard–sample bracketing was used to correct for instrumental mass bias. Samples and standard solutions were doped with NIST SRM 981 Pb, and the Pb (24 ng g^{-1}) and Tl (2 ng g^{-1}) concentrations were matched for the sample and standard solutions. The certified $^{208}Pb/^{206}Pb$ ratio was used to carry out an online correction for the instrumental mass bias of the $^{205}Tl/^{203}Tl$ ratio. The unknown samples were interspersed between analyses of NIST SRM 997. The Tl isotopic compositions are reported as the deviation of from the mass bias corrected $^{205}Tl/^{203}Tl$ ratio of the Tl isotope standard NIST SRM 997 (defined as $\varepsilon^{205}Tl_{SRM\ 997} = 0$) in parts per 10^4:

$$\varepsilon^{205}Tl_{NIST\ 997} = \left[\frac{\left(^{205}Tl/^{203}Tl\right)_{sample}}{\left(^{205}Tl/^{203}Tl\right)_{NIST\ SRM\ 997}} - 1\right] \times 10000$$

The results for the Fluka Tl standard solution were used to monitor data the accuracy and long-term precision.

3. Results and discussion

3.1. Distribution coefficient of Tl on TBP resin

The TBP extraction chromatography resin is an extractant of tributyl phosphate (TBP) that has been impregnated onto an inert polymeric substrate. It is a widely used organic phosphorus (P) neutral extractant in the nuclear and reprocessing industry (Aardaneh et al., 2008; Andris and Bena, 2016; Mikolajczak et al., 2019; Younes et al., 2020). The separation technique utilizes the two oxidation states of Tl. Oxidized Tl^{3+} is adsorbed much more strongly to the TBP resin than Tl^{+} in HCl. In this study, the extraction behavior of Tl^{3+} and Pb^{2+} on the TBP resin was investigated in order to establish a novel and simple Tl preconcentration method. Batch experiments were carried out to determine the distribution coefficients (K_d) of Tl^{3+} and Pb^{2+} on TBP resin in various concentrations of HCl, HNO_3, and aqua regia (the concentrations of HCl and HNO_3 were 0.1, 0.5, 1, and 2 M, and the concentrations of aqua regia were 5%, 10%, 15%, and 20% *v/v*). An aliquot (0.05 g) of the resin powder was immersed in 10 mL of each solution with 5 μg mL^{-1} of the target element (Tl or Pb) in a 15 mL centrifuge tube. The mixture was agitated for 4 h and then centrifuged. An aliquot from the aqueous phase was diluted in 2% HNO_3 and analyzed by ICP-MS.

For comparison, the distribution coefficients were defined with the same nomenclature as Younes et al. (2020) and calculated using the following equation:

$$K_d = \left(\frac{C_i - C_{aq}}{C_{aq}}\right) \times \left(\frac{V}{M_s}\right)$$

where C_i and C_{aq} are the aqueous phase concentration before and after resin contact in ng/mL, respectively, M_s is the resin mass in g, and V is the solution volume in mL.

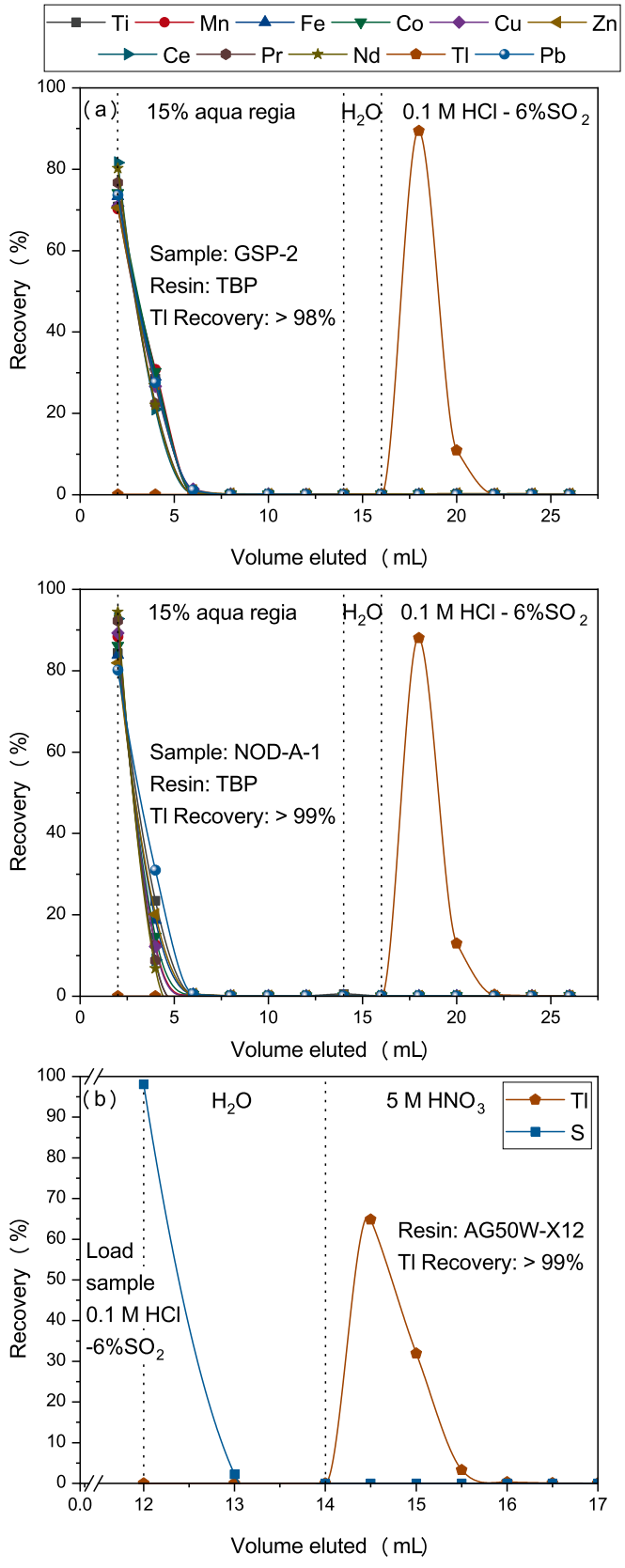

Fig. 3. (a) Elution curves for GSP-2 and NOD-A-1 of the TBP resin. (b) Elution curve of GSP-2 purified by TBP on AG50W-X12 cation exchange resin (NOD-A-1 is the same).

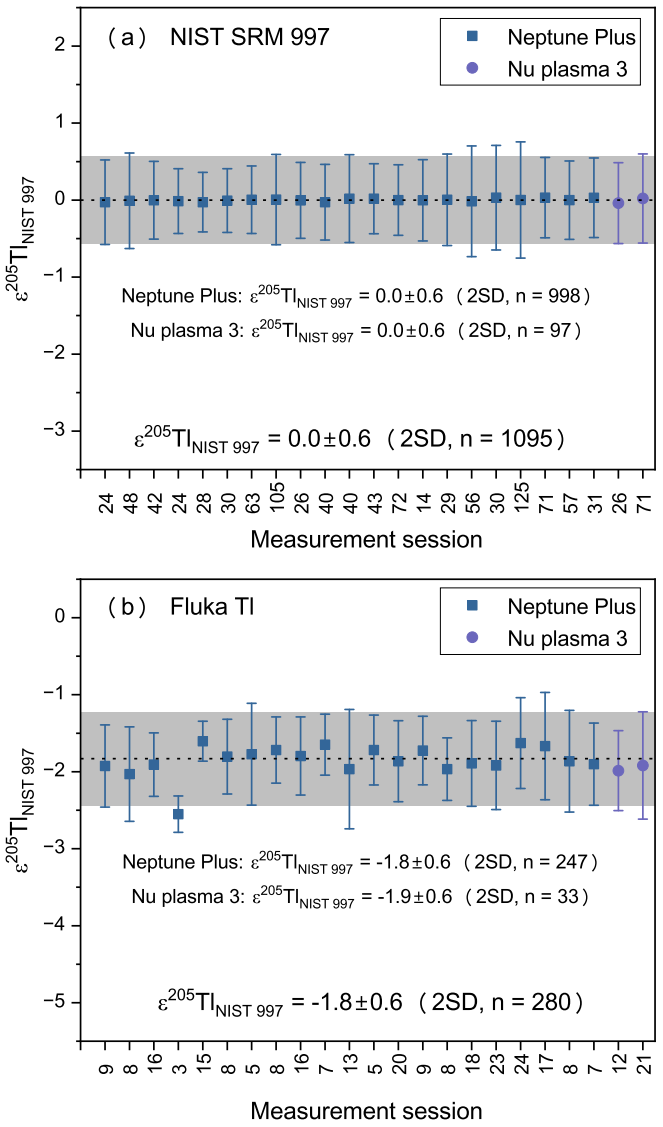

Fig. 4. Repeatability of Tl isotopic compositions ($\varepsilon^{205}Tl_{NIST\ 997}$ values) of NIST SRM 997 and Fluka Tl over the course of twenty-three measurement sessions. Each session is displayed as 1 point, the values of abscissa are the number of measurements made during each session, and the error bars indicate the precision (2SD, standard deviation) calculated from those measurements for each analytical session. The overall long-term measurement reproducibility is represented by the grey band (2SD, standard deviation).

The K_d results are shown in Fig. 2. In 5%–15% aqua regia, the K_d value of Tl^{3+} increased with increasing aqua regia concentration to a maximum of 1.8×10^5. However, the K_d value of Tl^{3+} dramatically decreased to 9.4×10^4 in 20% aqua regia. For the HCl medium, the K_d value of Tl^{3+} increased slightly from 5.9×10^3 to 7.2×10^3 over the investigated acidity range (0.1–2 M). In the HNO_3 medium, Tl^{3+} was not adsorbed to the resin ($K_d = 0$). The distribution coefficient for Tl^{3+} in aqua regia is 1–2 orders of magnitude higher than in the HCl medium. These results show that Tl^{3+} has the strongest adsorption capacity in 15% aqua regia. Based on the aqueous phase Tl concentration before and after resin contact, the exchange capacity of fresh TBP resin for Tl^{3+} was determined to be 1.00 mg g^{-1} in 15% aqua regia. In all the acid mediums, Pb was not adsorbed by the TBP resin (i.e., $K_d = 0$). These characteristics highlight the usefulness of the TBP resin for Tl separation.

Table 3
The $\varepsilon^{205}Tl_{NIST\ 997}$ for different geological reference materials. Relevant literature data are also listed.

Sample	Lithology	Origin	$\varepsilon^{205}Tl_{NIST\ 997}$ (2SD)	n	Instrument	[Tl][a] (ng g^{-1})
BHVO-2 (USGS)	Basalt	This Study	−1.6 ± 0.2	2	Neptune Plus	19 ± 3
			−1.4 ± 0.4	3	Nu plasma 3	20 ± 3
			−1.5 ± 0.4	5	mean	20 ± 3
		[b]Nielsen et al. (2017)	−1.8 ± 0.3	17		18
		Brett et al. (2018)	−1.2 ± 0.7	4		23 ± 1
		Gaschnig et al. (2021)	−1.78 ± 0.86	2		
BCR-2 (USGS)	Basalt	This Study	−2.4 ± 0.5	3	Neptune Plus	247 ± 30
			−2.1 ± 0.4	3	Nu plasma 3	249 ± 10
			−2.2 ± 0.5	6	mean	248 ± 21
		[b]Nielsen et al. (2017)	−2.5 ± 0.4	4		257
		Brett et al. (2018)	−2.4 ± 0.2	5		306 ± 21
		Gaschnig et al. (2021)	−2.24 ± 0.078	3		
AGV-2 (USGS)	Andesite	This Study	−2.6 ± 0.5	6	Neptune Plus	239 ± 31
			−2.4 ± 0.2	3	Nu plasma 3	233 ± 8
			−2.6 ± 0.4	9	mean	236 ± 22
		[b]Nielsen et al. (2017)	−3.0 ± 0.6	8		269
		Vaněk et al. (2018)	−3.2 ± 0.6	2		239
		Hettmann et al. (2014)	−2.7 ± 0.4	1		
GSP-2 (USGS)	Granodiorite	This Study	−2.3 ± 0.6	6	Neptune Plus	1315 ± 94
			−2 ± 0.2	3	Nu plasma 3	1281 ± 76
			−2.2 ± 0.6	9	mean	1298 ± 85
		Brett et al. (2018)	−2.5 ± 0.6	9		1500 ± 81
		Zhang et al. (2016)		3		1310 ± 150
COQ-1 (USGS)	Carbonate	This Study	−1.9 ± 0.4	5	Neptune Plus	79 ± 9
			−1.6 ± 0.2	3	Nu plasma 3	84 ± 4
			−1.8 ± 0.4	8	mean	82 ± 8
		Brett et al. (2018)	−2.3 ± 0.5	5		96 ± 4
NOD-P-1 (USGS)	Marine sediment	This Study	3.1 ± 0.5	2	Neptune Plus	160,000 ± 11,700
			3.4 ± 0.7	4	Nu plasma 3	154,000 ± 22,100
			3.3 ± 0.7	6	mean	156,000 ± 19,000
		Rehkämper et al. (2002)	0.5	1		146,000
NOD-A-1 (USGS)	Marine sediment	This Study	10.6 ± 0.8	4	Nu plasma 3	116,000 ± 20,800
		Rehkämper et al. (2002)	8.9	1		
		Nielsen et al. (2017)	10.7 ± 0.5	6		108,000
GSS-6 (IGGE)	Soil	This Study	−2.2 ± 0.2	3	Neptune Plus	2185 ± 81
SCo-1 (USGS)	Shale	This Study	−2.5 ± 0.3	3	Neptune Plus	715 ± 82
		Owens et al. (2017)	−2.5 ± 0.33	2		680 ± 86
		Ostrander et al. (2017)	−2.64 ± 0.24	9		

[a] The Tl mass fraction was estimated using MC-ICP-MS in this study, and the uncertainty were represented 2SD.
[b] Nielsen et al. (2017) compiled the results from Baker et al. (2009), Prytulak et al. (2013) and Coggon et al. (2014).

3.2. TBP resin separation of Tl

Quantitative and complete separation of Tl from samples is required for precise and accurate measurements of Tl stable isotope ratios by MC–ICP–MS. The elution behavior of Tl and matrix elements was investigated by using the two geological reference materials GSP-2 (granodiorite) and NOD-A-1 (Fe—Mn nodule). These materials were chosen instead of synthetic elemental mixtures because of their complex matrixes, which represent those of actual geological samples. Based on the distribution coefficient results, Tl^{3+} has a strong adsorption capacity on TBP resin in 15% aqua regia. As shown in Fig. 3, almost all elements, such as the major matrix elements (Ti, Mn, Fe), transition metals (Cu, Co, and Zn), rare earth elements (Ce, Pr, and Nd), and Pb were not retained by the TBP resin in 15% *v/v* aqua regia except for Tl. To avoid reaction of the residual aqua regia with the subsequent elution, 2 mL of ultrapure water was eluted. Finally, the Tl was eluted with 0.1 M HCl–6% *w/w* SO_2. In this stage, the Pb in the samples was completely separated from Tl. Previous studies have shown that 0.1 M HCl–5% *w/w* SO_2 solution can convert Tl to its univalent state for collection from anion ion-exchange resin (Brett et al., 2018; Nielsen et al., 2004; Rehkämper and Halliday, 1999). The Tl isotopic analytical artefacts can be up to 1 ε unit if H_2SO_4 is present in the samples but not in the bracketing standards (Nielsen et al., 2004). As such, we attempted to use reductive reagents such as ascorbic acid and hydrazine hydrochloride ($NH_2NH_2{\cdot}2HCl$) to strip Tl^{3+} from the TBP resin. However, low recoveries of Tl were obtained, which indicates these reagents do not fully reduce Tl^{3+} to Tl^{+}. However, 0.1 M HCl–6% *w/w* SO_2 effectively stripped all the Tl from the TBP resin, and thus was used later in this study.

3.3. AG50W-X12 resin separation of the sulfur compounds

Although the addition of H_2SO_4 to Tl standard solutions can eliminate the matrix effect induced by residual H_2SO_4 on the Tl isotopic measurements, we attempted to purify Tl from H_2SO_4. Both cation and anion ion-exchange resins have been shown to separate SO_4^{2-} from other elements (Craddock et al., 2008; Das et al., 2012; Sun et al., 2018; Wang and Becker, 2014). We used a column charged with 0.3 mL of the anion ion-exchange resin AG1-X8 (200–400 mesh; Muromac®) for the separation of sulfur compounds. By directly loading the 0.1 M HCl–6% *w/w* SO_2 containing the Tl from the first TBP resin column into the AG1-X8 resin, Tl^{+} was difficult to adsorb and anions such as SO_4^{2-} and HSO_3^{-} were retained on the AG1-X8 resin. However, the sulfur compounds still cannot completely separate from Tl due to the possibility of residual SO_2. To cleanly separate the Tl from sulfur compounds, the 0.1 M HCl–6% *w/w* SO_2 containing Tl was evaporated down to a few drops to convert all sulfur compounds into SO_4^{2-}, because during the evaporation process, SO_2 is volatilized or oxidized by O_2 in the air. This solution was then diluted with ultrapure water and loaded onto AG1-X8 resin, and the SO_4^{2-} was adsorbed and the Tl^{+} was eluted and collected. This method can completely separate sulfur compounds from Tl. However, the evaporation of the 0.1 M HCl–6% *w/w* SO_2 containing Tl has a risk of Pb contamination and is time consuming.

We also attempted to use AG50W-X12 cation ion-exchange resin to

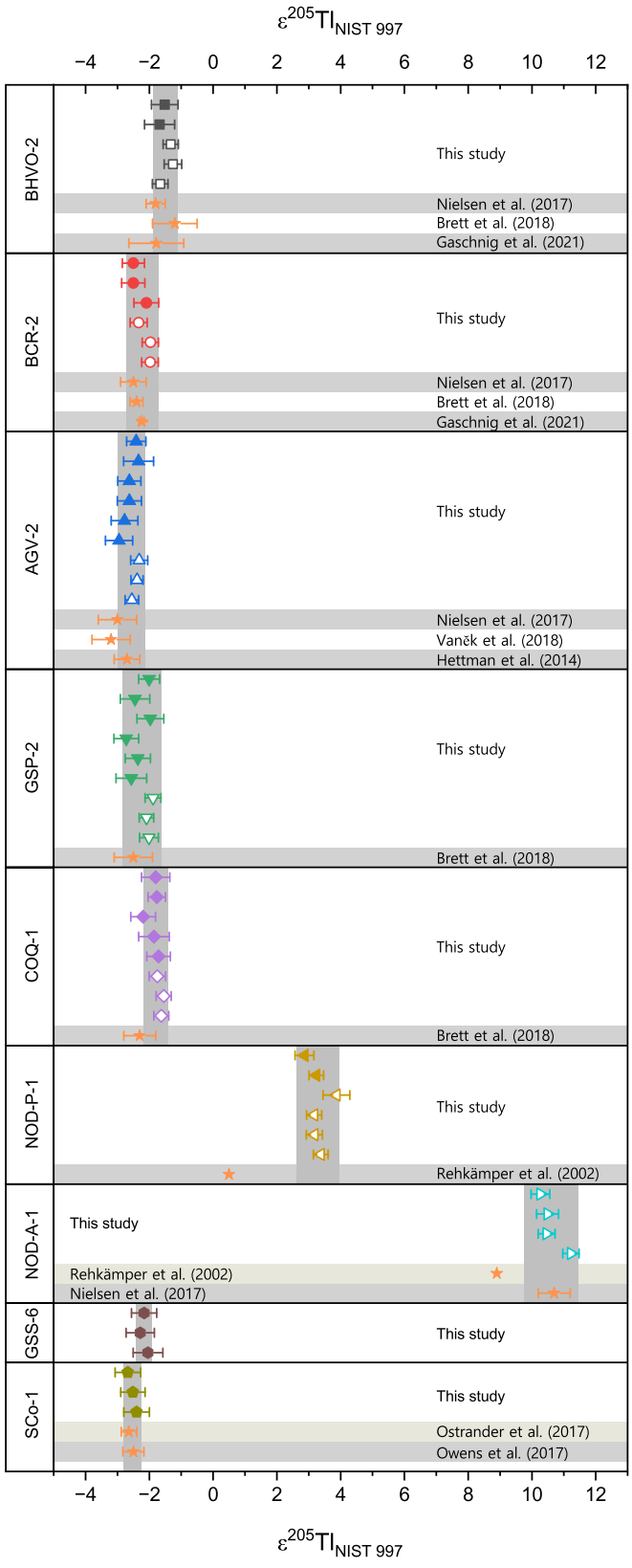

Fig. 5. The $\varepsilon^{205}Tl_{NIST\ 997}$ for different geological reference materials and comparison with literature. The $\varepsilon^{205}Tl_{NIST\ 997}$ value obtain from Nu plasma 3 is shown as unfilled symbol, Neptune Plus data are represented by filled symbol, and the literature data are shown as starlike symbol. Error bars reflect 2SE and the grey area represents 2SD of the $\varepsilon^{205}Tl_{NIST\ 997}$ value of the samples. Data are reported in Table 3.

remove the sulfur compounds. In 0.1 M HCl–6% *w/w* SO_2, Tl exists as Tl^+, while the sulfur compounds cannot exist in a cationic form. As shown in Fig. 3, the Tl^+ was completely adsorbed and the sulfur compounds were not retained by the AG50W-X12 resin in 0.1 M HCl-6% *w/w* SO_2. To elute the residual sulfur compounds, 2 mL of ultrapure water was added. The Tl^+ can be collected in 2 M HNO_3. To elute Tl faster and reduce the volume of the eluent, we used 5 M HNO_3 to collect Tl. This method not only completely removed sulfur compounds but also allowed the Tl eluent from the first column to be directly loaded onto AG50W-X12 resin without an evaporation step in the procedure. Therefore, we adopted a two-stage tandem column separation method for Tl using TBP and AG50W-X12 resins.

3.4. Recovery and blank

To assess the Tl recovery, geological reference materials (GSP-2, AGV-2, NOD-A-1, and NOD-P-1) were subjected to our Tl purification protocol. The recovery of Tl varied from 98.4% to 99.3%, with a mean value of 98.8% ± 0.8% (2SD; n = 4). The Tl procedural blank was evaluated by isotope dilution analysis, and was 1.57 ± 0.58 pg (2SD; n = 4), which is negligible compared to the sample Tl contents (> 10 ng).

3.5. Accuracy and precision

Prior to isotopic analysis of the samples, the Pb blank was determined from the m/z = 208 ion beam signal prior to addition of NIST SRM 981, and was <10 mV. The signal after Pb doping was $^{208}Pb > 10$ V. As such, the contribution of the Pb blank to the ^{208}Pb signal is insignificant. The effects of the Pb blank during Tl isotopic analysis can be evaluated by comparing the $^{207}Pb/^{206}Pb$ ratios (normalized to $^{208}Pb/^{206}Pb$ for the mass bias correction) of the samples and standard solutions in the same measurement sessions (Nielsen et al., 2004). In this study, for the Nu Plasma 3 instrument, the measurements were performed in two different analytical sessions. In the first session, the corrected results of the $^{207}Pb/^{206}Pb$ of the Tl standard solutions and samples are 0.91538 ± 0.00008 (2SD; n = 27) and 0.91538 ± 0.00002 (2SD; n = 2, samples) and, in the second session, the $^{207}Pb/^{206}Pb$ ratios are 0.91514 ± 0.00006 (2SD; n = 103; Tl standard solutions) and 0.91510 ± 0.00006 (2SD; n = 21; samples). For the Neptune Plus instrument, the $^{207}Pb/^{206}Pb$ are 0.91495 ± 0.00002 (2SD; n = 149; standard solutions) and 0.91496 ± 0.00005 (2SD; n = 24; samples), respectively. The $^{207}Pb/^{206}Pb$ ratios exhibit no significant difference between the standard solutions and samples, and residual Pb from the samples does not affect the Tl isotopic analyses.

In previous studies, an Alfa Aesar Tl standard solution was used to assess instrumental stability for >10 yr, and this standard has been measured on seven different instruments with a long-term error of 0.35 $\varepsilon^{205}Tl_{SRM\ 997}$ units (2SD, n = 187) (Nielsen et al., 2017). The reproducibility of our measurement procedure was evaluated by repeated analyses of two Tl standard solutions (NIST SRM 997 and Fluka Tl) using two different instruments (Neptune Plus and Nu Plasma 3). The $\varepsilon^{205}Tl_{SRM\ 997}$ value of NIST SRM 997 was 0.0 ± 0.6 (2SD; n = 998) using the Neptune Plus and 0.0 ± 0.6 (2SD; n = 97) using the Nu plasma 3. For the Fluka Tl standard, the Neptune Plus and Nu Plasma 3 instruments yielded $\varepsilon^{205}Tl_{SRM\ 997} = -1.8 \pm 0.6$ (2SD; n = 247) and − 1.9 ± 0.6 (2SD; n = 33), respectively. The long-term repeatability of $\varepsilon^{205}Tl_{SRM\ 997}$ values for the NIST SRM 997 and Fluka Tl solutions over six months was 0.0 ± 0.6 (2SD; n = 1095) and − 1.8 ± 0.6 (2SD; n = 280), respectively (Fig. 4). The results show that the Fluka Tl standard is a suitable standard solution for monitoring the stability of instruments, and that the two instruments can yield precise and accurate Tl isotopic values.

3.6. Analysis of reference materials

The applicability of our method for the analysis of natural samples was assessed by replicate analyses of seven geological reference

materials. These analyses included separate digestions of the reference material powders and column separations. Two instruments (Neptune Plus and Nu Plasma 3) were used to analyze the samples, and there were no significant differences between the measurements obtained with the two instruments. The results are reported in Table 3 and shown in Fig. 5.

The average $\varepsilon^{205}Tl_{SRM\ 997}$ values of six geological reference materials were found to be consistent with previously published data (Baker et al., 2009; Brett et al., 2018; Coggon et al., 2014; Gaschnig et al., 2021; Hettmann et al., 2014; Nielsen et al., 2017; Ostrander et al., 2017; Owens et al., 2017; Prytulak et al., 2013; Vaněk et al., 2018; Vaněk et al., 2021; Vaněk et al., 2020). The Tl isotopic composition of GSS-6 was measured for the first time, with $\varepsilon^{205}Tl_{SRM\ 997}$ values of -2.2 ± 0.2 (2SD, n = 3). We also determined the $\varepsilon^{205}Tl_{SRM\ 997}$ values of the Fe—Mn nodule NOD-A-1 and NOD-P-1, the results are 10.6 ± 0.8 (2SD; $n = 4$) and 3.3 ± 0.7 (2SD; $n = 6$), respectively. For NOD-A-1, the results are consistent with that reported by Nielsen et al. (2004) of 10.7 ± 0.5 (2SD; n = 6). However, these values are slightly higher than those of Rehkämper et al. (2002) (i.e., $\varepsilon^{205}Tl_{SRM\ 997}$ values for NOD-A-1 and NOD-P-1 of 8.9 and 0.5, respectively), which are based on a single analysis of each nodule standard. This difference may be due to the limited number of analyses obtained by Rehkämper et al. (2002). Nielsen et al. (2004) also proposed that this might be caused by different sample dissolution techniques. In this study, the Fe—Mn nodules were dissolved for 2–3 d in 6 M HCl on a hotplate at 120 °C, whereas Rehkämper et al. (2002) leached sample powders in 6 M HCl for only 15–30 min on a warm hotplate. This might explain the slight differences in the Tl isotopic compositions.

4. Conclusions

A two-stage tandem column procedure for the separation and purification of Tl from different geological reference materials was developed using TBP resin (50–100 μm) and AG50W-X12 cation ion-exchange resin (200–400 mesh). This separation procedure takes advantage of the separation of Tl from the matrix and interfering elements by TBP resin because Tl^{3+} has a strong affinity for TBP resin, unlike other elements, especially Pb. Further purification of Tl^{+} from SO_4^{2-} was undertaken by cation ion-exchange resin (AG50W-X12). The Tl isotopic measurements were undertaken by MC–ICP–MS (Neptune Plus and Nu Plasma 3) utilizing sample–standard bracketing with the NIST SRM 997 Tl standard and internal normalization by doping with the NIST SRM 981 Pb standard. The data accuracy and precision were evaluated by repeated measurements of the pure Fluka Tl standard solution, which yielded a long-term external reproducibility of better than ±0.6 with a mean $\varepsilon^{205}Tl_{SRM\ 997}$ value of −1.8 (2SD; $n = 280$). Analysis of nine different reference materials shows that our method can be effectively applied to a wide range of geological materials and yields precise and accurate results.

Declaration of Competing Interest

The authors declare that they have no known competing financial interests or personal relationships that could have appeared to influence the work reported in this paper.

Data availability

Data will be made available on request.

Acknowledgement

The helpful and constructive comments of three anonymous reviewers together with diligent editorial handing by Prof. Michael Ernst Böttcher substantially improved the manuscript and are greatly appreciated.

We thank Wenchang Wu of Guizhou Tongwei Analytical Technology Co., Ltd. For conducting the Tl isotope separation and analysis. This research was funded by the National Key Research and Development Project of China (2020YFA0714801) and Guizhou Provincial Science and Technology Project (No. [2020] 3Y003). This is contribution No. IS-3339 from GIGCAS.

References

Aardaneh, K., Saal, D., Swarts, G., Dewindt, S.C., 2008. TBP and TBP impregnated. Amberlite XAD-4 resin for radiochemical separation of Y-88 from Sr and Al. J. Radioanal. Nucl. Chem. 275 (3), 665–669.
Andris, B., Bena, J., 2016. The development of Sn-126 separation procedure by means of TBP resin. J. Radioanal. Nucl. Chem. 308 (3), 781–788.
Baker, R.G.A., Rehkämper, M., Hinkley, T.K., Nielsen, S.G., Toutain, J.P., 2009. Investigation of thallium fluxes from subaerial volcanism-Implications for the present and past mass balance of thallium in the oceans. Geochim. Cosmochim. Acta 73 (20), 6340–6359.
Bigeleisen, J., Mayer, M.G., 1947. Calculation of equilibrium constants for isotopic exchange reactions. J. Chem. Phys. 15 (5), 261–267.
Brett, A., Prytulak, J., Hammond, S.J., Rehkämper, M., 2018. Thallium Mass Fraction and Stable Isotope Ratios of Sixteen Geological Reference Materials. Geostand. Geoanal. Res. 42 (3), 339–360.
Coggon, R.M., et al., 2014. Controls on thallium uptake during hydrothermal alteration of the upper ocean crust. Geochim. Cosmochim. Acta 144, 25–42.
Craddock, P.R., Rouxel, O.J., Ball, L.A., Bach, W., 2008. Sulfur isotope measurement of sulfate and sulfide by high-resolution MC-ICP-MS. Chem. Geol. 253 (3–4), 102–113.
Das, A., Chung, C.H., You, C.F., Shen, M.L., 2012. Application of an improved ion exchange technique for the measurement of delta S-34 values from microgram quantities of sulfur by MC-ICPMS. J. Anal. At. Spectrom. 27 (12), 2088–2093.
Feldman, J., Levisohn, D.R., 1993. Acute alopecia-clue to thallium toxicity. Pediatr. Dermatol. 10 (1), 29–31.
Gaschnig, R.M., et al., 2021. Behavior of the Mo, Tl, and U isotope systems during differentiation in the Kilauea Iki lava lake. Chem. Geol. 574, 11.
Hettmann, K., et al., 2014. The geochemistry of Tl and its isotopes during magmatic and hydrothermal processes: the peralkaline Ilimaussaq complex, southwest Greenland. Chem. Geol. 366, 1–13.
Howarth, S., Prytulak, J., Little, S.H., Hammond, S.J., Widdowson, M., 2018. Thallium concentration and thallium isotope composition of lateritic terrains. Geochim. Cosmochim. Acta 239, 446–462.
Jones, J.H., Hart, S.R., Benjamin, T.M., 1993. Experimental partitioning studies near the Fe-FeS eutectic, with an emphasis on elements important to iron meteorite chronologies (Pb, Ag, Pd, and Tl). Geochim. Cosmochim. Acta 57 (2), 453–460.
Karbowska, B., 2016. Presence of thallium in the environment: sources of contaminations, distribution and monitoring methods. Environ. Monit. Assess. 188 (11), 19.
Kazantzis, G., 2000. Thallium in the environment and health effects. Environ. Geochem. Health 22 (4), 275–280.
Kersten, M., et al., 2014. Tracing anthropogenic thallium in soil using stable isotope compositions. Environ. Sci. Technol. 48 (16), 9030–9036.
Kiseeva, E.S., Wood, B.J., 2013. A simple model for chalcophile element partitioning between sulphide and silicate liquids with geochemical applications. Earth Planet. Sci. Lett. 383, 68–81.
Liu, J., et al., 2017. Thallium contamination in arable soils and vegetables around a steel plant a newly-found significant source of Tl pollution in South China. Environ. Pollut. 224, 445–453.
Liu, J., et al., 2020. Thallium isotopic fractionation in industrial process of pyrite smelting and environmental implications. J. Hazard. Mater. 384, 11.
Mikolajczak, R., et al., 2019. Scandium-47 separation by extraction chromatography using TBP resin. Journal of Labelled Compounds & Radiopharmaceuticals 62, S571–S572.
Nielsen, S.G., Rehkämper, M., Baker, J., Halliday, A.N., 2004. The precise and accurate determination of thallium isotope compositions and concentrations for water samples by MC-ICPMS. Chem. Geol. 204 (1–2), 109–124.
Nielsen, S.G., Rehkämper, M., Halliday, A.N., 2006a. Large thallium isotopic variations in iron meteorites and evidence for lead-205 in the early solar system. Geochim. Cosmochim. Acta 70 (10), 2643–2657.
Nielsen, S.G., Rehkämper, M., Norman, M.D., Halliday, A.N., Harrison, D., 2006b. Thallium isotopic evidence for ferromanganese sediments in the mantle source of Hawaiian basalts. Nature 439 (7074), 314–317.
Nielsen, S.G., et al., 2007. Thallium isotopes in Iceland and Azores lavas - Implications for the role of altered crust and mantle geochemistry. Earth Planet. Sci. Lett. 264 (1–2), 332–345.
Nielsen, S.G., et al., 2011. Thallium isotopes in early diagenetic pyrite - a paleoredox proxy? Geochim. Cosmochim. Acta 75 (21), 6690–6704.
Nielsen, S.G., Shimizu, N., Lee, C.T.A., Behn, M.D., 2014. Chalcophile behavior of thallium during MORB melting and implications for the sulfur content of the mantle. Geochemistry Geophysics Geosystems 15 (12), 4905–4919.
Nielsen, S.G., Klein, F., Kading, T., Blusztajn, J., Wickham, K., 2015. Thallium as a tracer of fluid-rock interaction in the shallow Mariana forearc. Earth Planet. Sci. Lett. 430, 416–426.
Nielsen, S.G., Rehkämper, M., Prytulak, J., 2017. Investigation and Application of Thallium Isotope Fractionation. In: Teng, F.Z., Watkins, J., Dauphas, N. (Eds.), Non-Traditional Stable Isotopes. Reviews in Mineralogy & Geochemistry. Mineralogical Soc Amer & Geochemical Soc, Chantilly, pp. 759–798.

Ostrander, C.M., Owens, J.D., Nielsen, S.G., 2017. Constraining the rate of oceanic deoxygenation leading up to a Cretaceous Oceanic Anoxic Event (OAE-2: similar to 94 Ma). Sci. Adv. 3 (8), 5.
Ostrander, C.M., et al., 2019. Fully oxygenated water columns over continental shelves before the Great Oxidation Event (vol 12, pg 186, 2019). Nat. Geosci. 12 (4), 307.
Owens, J.D., Nielsen, S.G., Horner, T.J., Ostrander, C.M., Peterson, L.C., 2017. Thallium-isotopic compositions of euxinic sediments as a proxy for global manganese-oxide burial. Geochim. Cosmochim. Acta 213, 291–307.
Peter, A.L.J., Viraraghavan, T., 2005. Thallium: a review of public health and environmental concerns. Environ. Int. 31 (4), 493–501.
Prytulak, J., Nielsen, S.G., Plank, T., Barker, M., Elliott, T., 2013. Assessing the utility of thallium and thallium isotopes for tracing subduction zone inputs to the Mariana arc. Chem. Geol. 345, 139–149.
Rehkämper, M., Halliday, A.N., 1999. The precise measurement of Tl isotopic compositions by MC-ICPMS: Application to the analysis of geological materials and meteorites. Geochim. Cosmochim. Acta 63 (6), 935–944.
Rehkämper, M., et al., 2002. Thallium isotope variations in seawater and hydrogenetic, diagenetic, and hydrothermal ferromanganese deposits. Earth Planet. Sci. Lett. 197 (1–2), 65–81.
Rehkämper, M., Frank, M., Hein, J.R., Halliday, A., 2004. Cenozoic marine geochemistry of thallium deduced from isotopic studies of ferromanganese crusts and pelagic sediments. Earth Planet. Sci. Lett. 219 (1–2), 77–91.
Shaw, D.M., 1952. The geochemistry of thallium. Geochim. Cosmochim. Acta 2 (2), 118–154.
Sun, S.L., Li, J., Zhang, L., Yin, L., Zhang, J., 2018. Simultaneous measurement of Re-Os and S isotopic compositions of sulfur-bearing minerals using a Carius tube digestion-based N-TIMS and MC-ICP-MS approach. J. Anal. At. Spectrom. 33 (6), 1057–1067.
Vaněk, A., et al., 2009. Lithogenic thallium behavior in soils with different land use. J. Geochem. Explor. 102 (1), 7–12.
Vaněk, A., et al., 2016. Isotopic Tracing of Thallium Contamination in Soils Affected by Emissions from Coal-Fired Power Plants. Environ. Sci. Technol. 50 (18), 9864–9871.
Vaněk, A., et al., 2018. Thallium isotopes in metallurgical wastes/contaminated soils: a novel tool to trace metal source and behavior. J. Hazard. Mater. 343, 78–85.
Vaněk, A., et al., 2020. Thallium stable isotope ratios in naturally Tl-rich soils. Geoderma 364.
Vaněk, A., et al., 2021. Thallium and lead variations in a contaminated peatland: a combined isotopic study from a mining/smelting area. Environ. Pollut. 290, 9.
Vejvodová, K., et al., 2020. Thallium isotopic fractionation in soil: the key controls. Environ. Pollut. 265 (PT A), 7.
Vejvodová, K., Vaněk, A., Drabek, O., Spasic, M., 2022. Understanding stable Tl isotopes in industrial processes and the environment: a review. J. Environ. Manag. 315, 10.
Voegelin, A., et al., 2015. Thallium speciation and extractability in a thallium- and arsenic-rich soil developed from mineralized carbonate rock. Environ. Sci. Technol. 49 (9), 5390–5398.
Wang, Z.C., Becker, H., 2014. Abundances of sulfur, selenium, tellurium, rhenium and platinum-group elements in eighteen reference materials by isotope dilution sector-field ICP-MS and negative TIMS. Geostand. Geoanal. Res. 38 (2), 189–209.
Wang, X.L., Zhang, L., Zhao, Z.H., Cai, Y.J., 2018. Heavy metal pollution in reservoirs in the hilly area of southern China: distribution, source apportionment and health risk assessment. Sci. Total Environ. 634, 158–169.
Wang, Y., Bodin, S., Blusztajn, J.S., Ullmann, C., Nielsen, S.G., 2022a. Orbitally paced global oceanic deoxygenation decoupled from volcanic CO2 emission during the middle Cretaceous Oceanic Anoxic Event 1b (Aptian-Albian transition). Geology 50 (11), 1324–1328.
Wang, Y., Lu, W., Costa, K.M., Nielsen, S.G., 2022b. Beyond anoxia: Exploring sedimentary thallium isotopes in paleo-redox reconstructions from a new core top collection. Geochim. Cosmochim. Acta 333 (15), 347–361.
Wood, B.J., Nielsen, S.G., Rehkamper, M., Halliday, A.N., 2008. The effects of core formation on the Pb- and Tl- isotopic composition of the silicate Earth. Earth Planet. Sci. Lett. 269 (3–4), 325–335.
Xiao, T.F., Guha, J., Boyle, D., 2004. High thallium content in rocks associated with Au-As-Hg-Tl and coal mineralization and its adverse environmental potential in SW Guizhou, China. Geochemistry-Exploration Environment Analysis 4, 243–252.
Xu, F.J., et al., 2018. Reassessment of heavy metal pollution in riverine sediments of Hainan Island, China: sources and risks. Environ. Sci. Pollut. Res. 25 (2), 1766–1772.
Younes, A., et al., 2020. Production of polonium from bismuth and purification using TBP resin and Sr resin. J. Radioanal. Nucl. Chem. 324 (2), 823–828.